

A Universal Density Matrix Functional from Molecular Orbital-Based Machine Learning: Transferability across Organic Molecules

Lixue Cheng,¹ Matthew Welborn,¹ and Thomas F. Miller III^{1, a)}

Division of Chemistry and Chemical Engineering, California Institute of Technology, Pasadena, CA 91125, USA

(Dated: 9 February 2024)

We address the degree to which machine learning can be used to accurately and transferably predict post-Hartree-Fock correlation energies. After presenting refined strategies for feature design and selection, the molecular-orbital-based machine learning (MOB-ML) method is first applied to benchmark test systems. It is shown that the total electronic energy for a set of 1000 randomized geometries of water can be described to within 1 millihartree using a model that is trained at the level of MP2, CCSD, or CCSD(T) using only a single reference calculation at a randomized geometry. To explore the breadth of chemical diversity that can be described, the MOB-ML method is then applied to a set of 7211 organic models with up to seven heavy atoms. It is shown that MP2 calculations on only 90 molecules are needed to train a model that predicts MP2 energies to within 2 millihartree accuracy for the remaining 7121 molecules; likewise, CCSD(T) calculations on only 150 molecules are needed to train a model that predicts CCSD(T) energies for the remaining molecules to within 2 millihartree accuracy. The MP2 model, trained with only 90 reference calculations on seven-heavy-atom molecules, is then applied to a diverse set of 1000 thirteen-heavy-atom organic molecules, demonstrating transferable preservation of chemical accuracy.

Machine learning (ML) has recently seen wide application in chemistry, including in the fields of drug discovery,^{1–3} materials design,^{4–7} and reaction prediction.^{8–12} In the context of quantum chemistry, much work has focused on predicting electronic energies or densities based on atom- or geometry-specific features,^{13–33} although other strategies have also been employed.³⁴ Recently, we reported an accurate and transferable molecular-orbital-based machine learning (MOB-ML) approach to the prediction of correlated wavefunction energies based on input features from a self-consistent field calculation, such as the Hartree-Fock method.³⁵ In this communication, we present refinements to the MOB-ML method with comparisons to test cases from our previous work. We then demonstrate the performance of MOB-ML across a broad swath of chemical space, as represented by the QM7b³⁶ and GDB-13³⁷ test sets of organic molecules.

I. THEORY

The current work aims to predict post-Hartree-Fock correlated wavefunction energies using features of the Hartree-Fock molecular orbitals (MOs). The starting point for the MOB-ML method³⁵ is that the correlation energy can be decomposed into pairwise occupied MO contributions^{38,39}

$$E_c = \sum_{ij}^{\text{occ}} \epsilon_{ij}, \quad (1)$$

where the pair correlation energy ϵ_{ij} can be written as a functional of the full set of MOs, $\{\phi_p\}$, appropriately indexed by i and j

$$\epsilon_{ij} = \mathcal{E}[\{\phi_p\}^{ij}]. \quad (2)$$

The functional \mathcal{E} is universal across all chemical systems; for a given level of correlated wavefunction theory, there is a corresponding \mathcal{E} that maps the HF MOs to the pair correlation energy, regardless of the molecular composition or geometry. Furthermore, \mathcal{E} simultaneously describes the pair correlation energy for all pairs of occupied MOs (i.e., the functional itself does not depend on i and j). For example, in second-order Møller-Plessett perturbation theory (MP2),⁴⁰ the pair correlation energies are

$$\epsilon_{ij}^{\text{MP2}} = \frac{1}{4} \sum_{ab}^{\text{virt}} \frac{|\langle ij|ab \rangle|^2}{e_a + e_b - e_i - e_j} \quad (3)$$

where a and b index virtual MOs, e_p is the Hartree-Fock orbital energy corresponding to MO ϕ_p , and $\langle ij|ab \rangle$ are antisymmetrized electron repulsion integrals.³⁹ A corresponding expression for the pair correlation energy exists for any post-Hartree-Fock method, but it is typically costly to evaluate in closed form.

In MOB-ML, a machine learning model is constructed for the pair energy functional

$$\epsilon_{ij} \approx \mathcal{E}^{\text{ML}}[\mathbf{f}_{ij}] \quad (4)$$

where \mathbf{f}_{ij} denotes a vector of features associated with MOs i and j . Eq. 4 thus presents the opportunity for the machine learning of a universal density matrix functional for correlated wavefunction energies, which can be evaluated at the cost of the MO calculation.

Following our previous work,³⁵ the features \mathbf{f}_{ij} correspond to unique elements of the Fock (**F**), Coulomb (**J**), and exchange (**K**) matrices between ϕ_i , ϕ_j , and the set of virtual orbitals. In the current work, we additionally include features associated with matrix elements between pairs of occupied orbitals for which one member of the pair differs from ϕ_i or ϕ_j (i.e., non- i,j occupied MO pairs). The feature vector takes the

^{a)}Electronic mail: tfm@caltech.edu.

form

$$\mathbf{f}_{ij} = (F_{ii}, F_{ij}, F_{jj}, \mathbf{F}_i^o, \mathbf{F}_j^o, \mathbf{F}_{ij}^{vv}, \\ J_{ii}, J_{ij}, J_{jj}, \mathbf{J}_i^o, \mathbf{J}_j^o, \mathbf{J}_{ij}^{vv}, \\ K_{ij}, \mathbf{K}_i^o, \mathbf{K}_j^o, \mathbf{K}_i^v, \mathbf{K}_j^v, \mathbf{K}_{ij}^{vv}). \quad (5)$$

where the superscript o denotes a row of the occupied–occupied block, the superscript v denotes a row of the occupied–virtual block, and the superscript vv denotes the virtual–virtual block. To increase transferability and accuracy, we choose ϕ_i and ϕ_j to be localized molecular orbitals (LMOs) rather than canonical MOs and employ valence virtual LMOs⁴¹ in place of the set of all virtual MOs (as detailed in Ref. 35). We separate Eq. 4 to independently machine learn the cases of $i = j$ and $i \neq j$,

$$\epsilon_{ij} \approx \begin{cases} \epsilon_d^{\text{ML}}[\mathbf{f}_i] & \text{if } i = j \\ \epsilon_o^{\text{ML}}[\mathbf{f}_{ij}] & \text{if } i \neq j \end{cases} \quad (6)$$

where \mathbf{f}_i denotes \mathbf{f}_{ii} (Eq. 5) with redundant elements removed; by separating the pair energies in this way, we avoid the situation where a single ML model is required to distinguish between the cases of $i = j$ and ϕ_i being nearly degenerate to ϕ_j , a distinction which can represent a sharp variation in the function to be learned.

In the current work, several technical refinements are introduced to improve training efficiency (i.e., the accuracy and transferability of the model as a function of the number of training examples). These are now described.

Occupied LMO symmetrization. The feature vector is pre-processed to specify a canonical ordering of the occupied and virtual LMO pairs. This reduces permutation of elements in the feature vector, resulting in greater ML training efficiency. Matrix elements M_{ij} ($\mathbf{M} = \mathbf{F}, \mathbf{J}, \mathbf{K}$) associated with ϕ_i and ϕ_j are rotated into gerade and ungerade combinations

$$\begin{aligned} M_{ii} &\leftarrow \frac{1}{2}M_{ii} + \frac{1}{2}M_{jj} + M_{ij} \\ M_{jj} &\leftarrow \frac{1}{2}M_{ii} + \frac{1}{2}M_{jj} - M_{ij} \\ M_{ij} &\leftarrow \frac{1}{2}M_{ii} - \frac{1}{2}M_{jj} \\ M_{ip} &\leftarrow \frac{1}{\sqrt{2}}M_{ip} + \frac{1}{\sqrt{2}}M_{jp} \\ M_{jp} &\leftarrow \frac{1}{\sqrt{2}}M_{ip} - \frac{1}{\sqrt{2}}M_{jp} \end{aligned} \quad (7)$$

with the sign convention that F_{ij} is negative. Here, p indexes either one of the occupied LMOs other than i and j or one of the virtual LMOs.

LMO sorting. The virtual LMO pairs are sorted by increasing distance from occupied orbitals ϕ_i and ϕ_j . The distance is defined as

$$R_a^{ij} = \|\langle \phi_i | \hat{R} | \phi_i \rangle - \langle \phi_a | \hat{R} | \phi_a \rangle\| + \|\langle \phi_j | \hat{R} | \phi_j \rangle - \langle \phi_a | \hat{R} | \phi_a \rangle\|, \quad (8)$$

where ϕ_a is a virtual LMO, \hat{R} is the Cartesian position operator, and $\|\cdot\|$ denotes the 2-norm. Previously,³⁵ distances were

defined based on Coulomb repulsion, which can lead to inconsistent sorting for systems with strongly polarized bonds. We recognize this issue could also potentially be addressed through the use of symmetry functions,⁴² but these are not employed in the current work. The non- i, j occupied LMO pairs are sorted in the same manner as the virtual LMO pairs.

Orbital localization. We employ Boys localization⁴³ to obtain the occupied LMOs, rather than the IBO localization⁴¹ employed in our previous work.³⁵ Particularly for molecules that include triple bonds or multiple lone pairs, it is found that Boys localization provides more consistent localization as a function of small geometry changes than IBO localization; and the chemically unintuitive mixing of σ and π bonds in Boys localization (“banana bonds”)⁴⁴ does not present a problem for the MOB-ML method.

Feature selection. Prior to training, automatic feature selection is performed using random forest regression⁴⁵ with the mean decrease of accuracy criterion (sometimes called permutation importance).⁴⁶ This technique was found to be more effective than our previous use³⁵ of the Gini importance score.⁴⁵

II. COMPUTATIONAL DETAILS

Results are presented for a single water molecule, a series of alkane molecules, the QM7b set³⁶ of 7211 molecules with up to seven C, O, N, S, and Cl heavy atoms, and a randomly selected subset of 1000 molecules from the GDB-13 set³⁷ of molecules with thirteen C, O, N, S, and Cl heavy atoms.

Training and test geometries are sampled at 50 fs intervals from *ab initio* molecular dynamics trajectories performed with the Q-CHEM 5.0 software package,⁴⁷ using the B3LYP^{48–51}/6-31g*⁵² level of theory and a Langevin thermostat⁵³ at 350 K.

The features and training pair energies associated with these geometries are computed using the MOLPRO 2018.0 software package⁵⁴ in a cc-pVTZ basis set unless otherwise noted.⁵⁵ Valence virtual orbitals used in feature construction are determined with the Intrinsic Bond Orbital method.⁴¹ Reference pair correlation energies are computed with second-order Møller-Plessett perturbation theory (MP2)^{40,56} and coupled cluster with singles and doubles (CCSD)^{57,58} as well as with perturbative triples [CCSD(T)].^{59,60} Density fitting for both Coulomb and exchange integrals⁶¹ is employed for all results below except those corresponding to the water molecule. The frozen core approximation is used in all cases.

Gaussian process regression (GPR)⁶² is employed to machine learn ϵ_d^{ML} and ϵ_o^{ML} (Eq. 6) using the GPY 1.9.6 software package.⁶³ The GPR kernel is Matérn 5/2 with white noise regularization.⁶² Kernel hyperparameters are optimized with respect to the log marginal likelihood objective for the water and alkane series results, as well as for ϵ_d^{ML} of the QM7b results. We use the Matérn 3/2 kernel instead of the Matérn 5/2 kernel for the case of ϵ_o^{ML} for QM7b results, as it was empirically found to yield slightly better accuracy.⁶⁴

Feature selection is performed using the random forest regression implementation in the SCIKIT-LEARN v0.20.0 package.⁶⁵

III. RESULTS

The ML model of Eq. 6 is a universal functional for any molecular Hamiltonian. In principle, with an adequate feature list and unlimited training data (and time), it should accurately describe all molecular systems. In practice, we must train the ML model using a truncated feature list and finite data. These choices determine the accuracy of the model.

Below, we examine the performance of the MOB-ML method in three increasingly broad regions of chemical space: (i) training on randomized water molecule geometries and predicting the energies of other water molecule geometries; (ii) training on geometries of short alkanes and predicting the energies of longer alkanes, and (iii) training on a small set of organic molecules and predicting the energies of a broader set of organic molecules. The first two test cases were introduced in our previous work,³⁵ and here we explore how the refined methodology reported in this work leads to improvements in accuracy and transferability. The last case represents a demanding new test of transferability across chemical space. In all cases, we report the ML prediction accuracy as a function of the number of training examples.

As a first example, we consider the performance of MOB-ML for a single water molecule. A separate model is trained to predict the correlation energy at the MP2, CCSD, and CCSD(T) levels of theory, using reference calculations on a subset of 1000 randomized water geometries to predict the correlation energy for the remainder. Feature selection with an importance threshold of 1×10^{-3} results in 12, 11 and 10 features for ϵ_o^{ML} for MP2, CCSD and CCSD(T), respectively; ten features are selected for ϵ_d^{ML} for all three post-Hartree-Fock methods.

Figure 1 presents the test set prediction accuracy of each MOB-ML model as a function of the number of training geometries (i.e., the “learning curve”). MOB-ML predictions are shown for MP2, CCSD, and CCSD(T), and the model shows the same level of accuracy for all three methods. Remarkably, all three models achieve a prediction mean absolute error (MAE) of 1 mH when trained on only a single water geometry, indicating that only a single reference calculation is needed to provide chemical accuracy for the remaining 999 geometries at each level of theory. Since it contains 10 distinct LMO pairs, this single geometry provides enough information to yield a chemically accurate MOB-ML model.

For all three methods, the learning curve exhibits the expected⁶⁶ power-law behavior as a function of training data, and the total error approaches microhartree accuracy with only ~ 10 training geometries of water. As compared to our previous results, where training on 200 geometries resulted in a prediction MAE of 0.027 mH for the case of CCSD,³⁵ the current implementation of the MOB-ML model is substantially improved; the improvement for this case stems primarily from the use of Boys localization,⁴³ which specifies unique and consistent LMOs corresponding to the oxygen lone pairs.

Next, we explore the transferability of MOB-ML predictions, for a model that is trained on the smallest alkanes (ethane and propane) and then used for predictions on larger and more branched alkanes (n-butane and isobutane). Specifi-

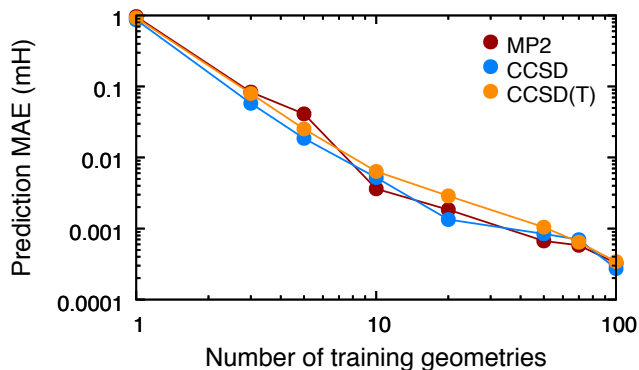


FIG. 1. Learning curves for MOB-ML models trained on the water molecule and used to predict the correlation energy of different water molecule geometries at three levels of post-Hartree-Fock theory. Prediction errors are summarized in terms of mean absolute error (MAE).

cally, we make predictions for n-butane and isobutane using a MOB-ML model trained using either 50 geometries of ethane (Fig. 2(a)) or 50 geometries of ethane and 20 geometries of propane (Fig. 2(b)). Features are selected with an importance threshold of 1×10^{-4} , resulting in (a) 23 features for ϵ_d^{ML} and 10 features for ϵ_o^{ML} , and (b) 27 features for ϵ_d^{ML} and 18 features for ϵ_o^{ML} .

Figure 2 presents the prediction errors for the two MOB-ML models. Training on ethane alone, MOB-ML achieves mean absolute errors of 1 mH for both n-butane and isobutane. After addition of 20 propane geometries to the training set, these errors are roughly halved to 0.38 and 0.42 mH, respectively. For these predictions, the absolute zero of energy is shifted for each molecule to compare relative energies on its potential energy surface (i.e., parallelity errors are removed). These shifts are reported in the figure caption; for no other results reported in the paper are parallelity errors removed.

Compared to our previous work,³⁵ the results in Fig. 2 demonstrate substantial improvements. First, the overall prediction accuracy is improved for all four summary statistics (inset in Fig. 2) despite substantial reduction in the number of training examples used. (Previously, 300 ethane and 50 propane training geometries were employed). Second, n-butane and isobutane are predicted with similar accuracy. Finally, the prediction errors are no longer skewed as a function of true correlation energy. The dominant methodological sources of these improvements are found to be the symmetrization of occupied orbitals (Eq. 7) and the improved feature selection methodology.

We now examine the transferability of the MOB-ML method across a broad swath of chemical space. Specifically, we consider the QM7b dataset,³⁶ which is comprised of 7,211 plausible organic molecules with 7 or fewer heavy atoms. The chemical elements in QM7b are limited to those likely to be found in drug-like compounds: C, H, O, N, S, and Cl. For this test case, the MOB-ML model is trained on a subset of QM7b molecules and used to predict the correlation energy of the remainder.

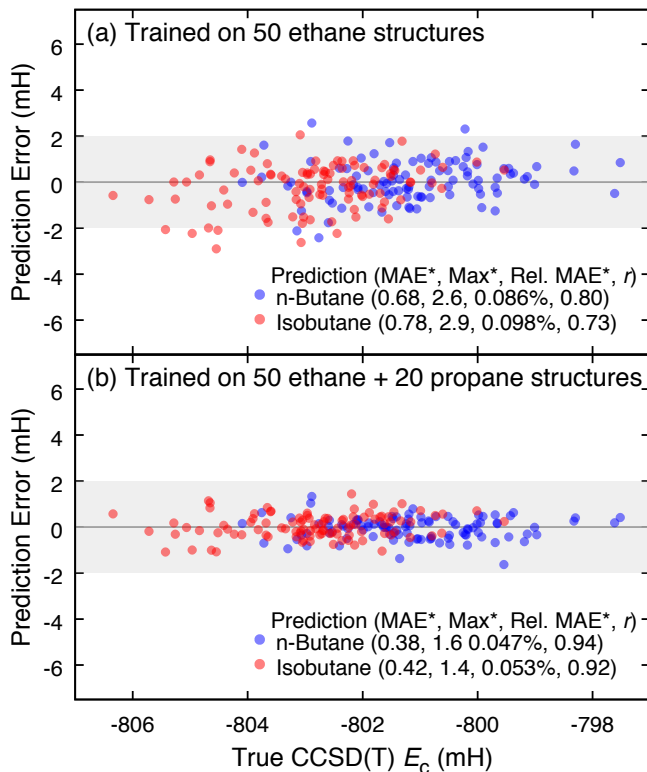


FIG. 2. MOB-ML predictions of the CCSD(T) correlation energy for n-butane and isobutane geometries, based on from training from (a) 50 ethane geometries and (b) 50 ethane and 20 propane geometries. MOB-ML prediction errors are plotted versus the true CCSD(T) correlation energy. To remove parallelity error, a global shift is applied to the predictions of n-butane and isobutane by (a) 10 and 15 mH and (b) 3.8 and 0.61 mH, respectively. Summary statistics that include this shift (indicated by an asterisk) are presented, consisting of mean absolute error (MAE*), maximum absolute error (Max*), MAE* as a percentage of E_c (Rel. MAE*), and Pearson correlation coefficient (r).⁶⁷ The gray shaded region corresponds to errors of ± 2 mH.

A possible source of concern in the MOB-ML technique is that the number of selected features would grow with the chemical complexity of the training data. For example, 27 features for ϵ_d^{ML} and 18 features for ϵ_o^{ML} were selected for the alkane test case using ethane + propane (Fig. 2), whereas only 10 features for ϵ_d^{ML} and 10 features for ϵ_o^{ML} were selected for the water test case at the CCSD(T) level of theory (Fig. 1). To examine this, we perform feature selection on increasing numbers of randomly selected molecules from the QM7b dataset. Table I presents two statistics on the feature importance as a function of the number of training molecules: (i) the number of “important features” (i.e., those whose permutation importance⁴⁶ exceeds a set threshold of 2×10^{-4} and 5×10^{-5} for ϵ_d^{ML} and ϵ_o^{ML} , respectively) and (ii) the inverse participation ratio⁶⁸ of the feature importance scores. The latter is a threshold-less measure of the number of important features; it takes a value of 1 when only 1 feature has nonzero importance and N when all N features have equal importance.

Although the QM7b dataset contains many different chemical elements and bonding motifs, Table I reveals that the selected features remain compact and do not grow with the number of training molecules. Indeed, for a large number of training molecules, the number of selected features slightly decreases, reaching 42 and 24 selected features for ϵ_d^{ML} and ϵ_o^{ML} , respectively, for the largest training sizes considered.

TABLE I. Number of features selected as a function of the number randomly chosen training molecules for the QM7b dataset at the CCSD(T)/cc-pVDZ level. The number of features that exceed an importance threshold as well as the inverse participation ratio (IPR) of the feature importance scores are reported (see text).

Training size	# of important features ϵ_d^{ML}	ϵ_o^{ML}	feature weight ϵ_d^{ML}	IPR ϵ_o^{ML}
20	50	28	4.720	1.116
50	46	28	3.718	1.097
100	46	26	3.450	1.115
200	42	24	3.430	1.120

In training the MOB-ML model on QM7b, we leverage the active learning capabilities of the GPR framework.⁶⁹ To begin, the model is trained using 20 randomly selected molecules. Then, the GPR uncertainty is computed for the remaining members of QM7b (without the need for a high-level calculation). The 10 molecules with the largest average GPR uncertainty—corresponding to the regions in feature space for which the MOB-ML model has the least information—for ϵ_o^{ML} are then added to the training set. The same set of training molecules is always employed for both ϵ_d^{ML} and ϵ_o^{ML} . At each active learning step, the initial guess for the kernel hyperparameters is taken to be the optimized hyperparameters from the previous step; the initial guess for the first step corresponds to hyperparameters of unity.

The resulting learning curves are shown in Fig. 3. Results are presented for MOB-ML models trained at the MP2/cc-pVTZ and CCSD(T)/cc-pVDZ levels of theory. The MOB-ML model achieves an accuracy of 2 mH with 90 and 150 training molecules (1.3% and 2.1% of the molecules in the QM7b dataset) for MP2 and CCSD(T), respectively. For MP2, an accuracy of 1 kcal/mol is reached with 210 training calculations. For comparison, Quantum Machine Learning (QML)—a kernel ridge regression based on features of molecular geometry—achieves the same accuracy at 2,048 training geometries (over 28% of the molecules in the QM7b dataset).⁷⁰ Also, presented for comparison is the 3-dimensional Combination QML (CQML) method⁷⁰ which employs a large number of low-level training calculations to improve model accuracy for a given number of high-level reference training calculations. While CQML shows potentially comparable accuracy to MOB-ML as a function of the number of high-level training calculations, it requires calculations at many intermediate levels of theory including 256 lowest-level training calculations per high-level calculation; for the QM7b dataset, there is insufficient data to train the CQML model beyond 28 high-level calculations, such that chemical accuracy is never reached in the results reported to date.⁷⁰

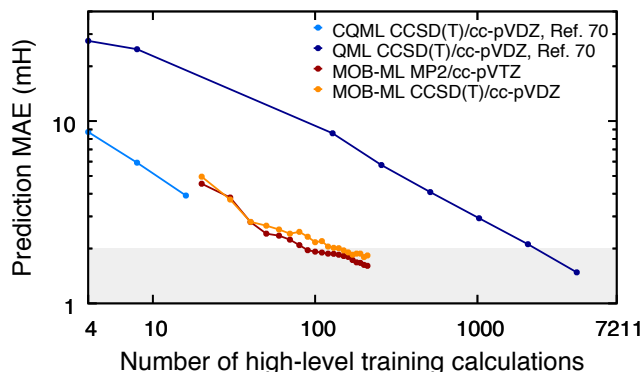


FIG. 3. MOB-ML learning curves for prediction of the QM7b dataset atomization energies at the MP2/cc-pVTZ (red) and CCSD(T)/cc-pVDZ (orange) levels of theory. The MOB-ML model is trained on a subset of QM7b molecules (as described in the text) and predictions are made for the remainder of the QM7b set. Quantum Machine Learning (QML, dark blue) and 3-dimensional Combination QML (CQML, light blue) results for the same test case are included for comparison.⁷⁰ The gray shaded area corresponds to errors of 2 mH.

As a final test of transferability of MOB-ML across chemical space, we take a MOB-ML model trained on QM7b and use it to predict 1,000 13-heavy-atom organic molecules chosen randomly from the GDB-13 dataset.³⁷ Like QM7b, the members of GDB-13 contain C, H, N, O, S, and Cl. The size of these molecules precludes the use of coupled cluster theory to generate reference data; we therefore make comparison at the MP2/cc-pVTZ level of theory, noting that MOB-ML has repeatedly been shown to provide similar prediction accuracy for all post-Hartree-Fock methods considered. Using the MOB-ML model for MP2 trained on 90 molecules (corresponding to a prediction MAE of 1.96 mH for QM7b), we observe a prediction MAE of 4.19 mH for the 1000 molecule sample of GDB-13. Expressed in terms of size-intensive quantities, the prediction MAE per heavy atom is 0.291 mH and 0.323 mH for QM7b and GDB-13, respectively, indicating that the accuracy of the MOB-ML results are only slightly when the model is applied to larger molecules. To further control the prediction accuracy, we take advantage of the ability of GPR to estimate the prediction uncertainty at negligible computational cost (i.e., without the need for high-level calculations). Exclusion of the 25% of GDB-13 molecules corresponding to the largest GPR uncertainties (i.e., restricting the predictions to the 750 13-heavy-atom molecules for which the model is most certain) results in a prediction MAE of 0.289 mH per heavy atom, which is in fact more accurate than the prediction MAE for the QM7B dataset.

IV. CONCLUSIONS

Molecular-orbital-based machine learning (MOB-ML) has been shown to be a simple and strikingly accurate strategy for predicting correlated wavefunction energies at the cost

of a Hartree-Fock calculation, benefiting from the intrinsic transferability of the localized molecular orbital representation. The starting point for the MOB-ML method is a rigorous mapping from the Hartree-Fock molecular orbitals to the total correlation energy, which ensures that the use of sufficient training data and molecular orbital features will produce a model that matches the corresponding correlated wavefunction method across the entirety of chemical space. The current work explores this possibility within the subspace of organic molecules. It is shown that MOB-ML can predict the QM7b dataset to within a 2 millihartree accuracy using only 90 MP2/cc-pVTZ and 150 CCSD(T)/cc-pVDZ training calculations. The prediction of the GDB-13 dataset using the MP2 model from 90 training calculations gives a similar error (0.323 mH per heavy atom) as it does for QM7b (0.291 mH per heavy atom), verifying the transferability of MOB-ML models across diverse sets of organic molecules. These results suggest that MOB-ML provides a promising approach toward the development of density matrix functionals that are applicable across broad swathes of chemical space.

ACKNOWLEDGMENTS

We thank Daniel Smith (Molecular Sciences Software Institute) and Alberto Gobbi (Genentech) for a helpful discussion about available training datasets. This work was supported by AFOSR award no. FA9550-17-1-0102. The authors additionally acknowledge support from the Resnick Sustainability Institute postdoctoral fellowship (MW) and the Camille Dreyfus Teacher-Scholar Award (TFM). This research also used resources of the National Energy Research Scientific Computing Center (NERSC), a DOE Office of Science User Facility supported by the DOE Office of Science under contract DE-AC02-05CH11231.

¹A. Laveccchia, "Machine-learning approaches in drug discovery: methods and applications," *Drug Discov. Today* **20**, 318–331 (2015).

²E. Gawehn, J. A. Hiss, and G. Schneider, "Deep learning in drug discovery," *Mol. Inform.* **35**, 3–14 (2016).

³M. Popova, O. Isayev, and A. Tropsha, "Deep reinforcement learning for de novo drug design," *Sci. Adv.* **4**, eaap7885 (2018).

⁴E. Kim, K. Huang, S. Jegelka, and E. Olivetti, "Virtual screening of inorganic materials synthesis parameters with deep learning," *npj Comput. Mater.* **3**, 53 (2017).

⁵F. Ren, L. Ward, T. Williams, K. J. Laws, C. Wolverton, J. Hattrick-Simpers, and A. Mehta, "Accelerated discovery of metallic glasses through iteration of machine learning and high-throughput experiments," *Sci. Adv.* **4**, eaag1566 (2018).

⁶K. T. Butler, D. W. Davies, H. Cartwright, O. Isayev, and A. Walsh, "Machine learning for molecular and materials science," *Nature* **559**, 547–555 (2018).

⁷B. Sanchez-Lengeling and A. Aspuru-Guzik, "Inverse molecular design using machine learning: Generative models for matter engineering," *Science* **361**, 360–365 (2018).

⁸J. N. Wei, D. Duvenaud, and A. Aspuru-Guzik, "Neural networks for the prediction of organic chemistry reactions," *ACS Cent. Sci.* **2**, 725–732 (2016).

⁹P. Raccuglia, K. C. Elbert, P. D. F. Adler, C. Falk, M. B. Wenny, A. Molloy, M. Zeller, S. A. Friedler, J. Schrier, and A. J. Norquist, "Machine-learning-assisted materials discovery using failed experiments," *Nature* **533**, 73–76 (2016).

- ¹⁰Z. W. Ulissi, A. J. Medford, T. Bligaard, and J. K. Nørskov, "To address surface reaction network complexity using scaling relations machine learning and DFT calculations," *Nat. Commun.* **8**, 14621 (2017).
- ¹¹M. H. S. Segler and M. P. Waller, "Neural-symbolic machine learning for retrosynthesis and reaction prediction," *Chem. - A Eur. J.* **23**, 5966–5971 (2017).
- ¹²M. H. S. Segler, M. Preuss, and M. P. Waller, "Planning chemical syntheses with deep neural networks and symbolic AI," *Nature* **555**, 604–610 (2018).
- ¹³J. S. Smith, O. Isayev, and A. E. Roitberg, "ANI-1: an extensible neural network potential with DFT accuracy at force field computational cost," *Chem. Sci.* **8**, 3192–3203 (2017).
- ¹⁴J. S. Smith, B. T. Nebgen, R. Zubatyuk, N. Lubbers, C. Devereux, K. Barros, S. Tretiak, O. Isayev, and A. Roitberg, "Outsmarting quantum chemistry through transfer learning," (2018).
- ¹⁵N. Lubbers, J. S. Smith, and K. Barros, "Hierarchical modeling of molecular energies using a deep neural network," *J. Chem. Phys.* **148**, 241715 (2018).
- ¹⁶A. P. Bartók, M. C. Payne, R. Kondor, and G. Csányi, "Gaussian approximation potentials: The accuracy of quantum mechanics, without the electrons," *Phys. Rev. Lett.* **104**, 136403 (2010).
- ¹⁷M. Rupp, A. Tkatchenko, K.-R. Müller, and O. A. von Lilienfeld, "Fast and accurate modeling of molecular atomization energies with machine learning," *Phys. Rev. Lett.* **108**, 58301 (2012).
- ¹⁸G. Montavon, M. Rupp, V. Gobre, A. Vazquez-Mayagoitia, K. Hansen, A. Tkatchenko, K.-R. Müller, and O. A. von Lilienfeld, "Machine learning of molecular electronic properties in chemical compound space," *New J. Phys.* **15**, 95003 (2013).
- ¹⁹K. Hansen, G. Montavon, F. Biegler, S. Fazli, M. Rupp, M. Scheffler, O. A. von Lilienfeld, A. Tkatchenko, and K.-R. Müller, "Assessment and validation of machine learning methods for predicting molecular atomization energies," *J. Chem. Theory Comput.* **9**, 3404 (2013).
- ²⁰P. Gasparotto and M. Ceriotti, "Recognizing molecular patterns by machine learning: an agnostic structural definition of the hydrogen bond," *J. Chem. Phys.* **141**, 174110 (2014).
- ²¹R. Ramakrishnan, P. O. Dral, M. Rupp, and O. A. von Lilienfeld, "Big data meets quantum chemistry approximations: the Δ -machine learning approach," *J. Chem. Theory Comput.* **11**, 2087 (2015).
- ²²J. Behler, "Perspective: Machine learning potentials for atomistic simulations," *J. Chem. Phys.* **145**, 170901 (2016).
- ²³S. Kearnes, K. McCloskey, M. Berndl, V. Pande, and P. Riley, "Molecular graph convolutions: moving beyond fingerprints," *J. Comput. Aided Mol. Des.* **30**, 595 (2016).
- ²⁴F. Paesani, "Getting the right answers for the right reasons: toward predictive molecular simulations of water with many-body potential energy functions," *Acc. Chem. Res.* **49**, 1844 (2016).
- ²⁵K. T. Schütt, F. Arbabzadah, S. Chmiela, K.-R. Müller, and A. Tkatchenko, "Quantum-chemical insights from deep tensor neural networks," *Nat. Commun.* **8**, 13890 (2017).
- ²⁶F. Brockherde, L. Vogt, L. Li, M. E. Tuckerman, K. Burke, and K.-R. Müller, "Bypassing the Kohn-Sham equations with machine learning," *Nat. Commun.* **8**, 872 (2017).
- ²⁷Z. Wu, B. Ramsundar, E. N. Feinberg, J. Gomes, C. Geniesse, A. S. Pappu, K. Leswing, and V. Pande, "MoleculeNet: a benchmark for molecular machine learning," *Chem. Sci.* **9**, 513 (2018).
- ²⁸T. T. Nguyen, E. Székely, G. Imbalzano, J. Behler, G. Csányi, M. Ceriotti, A. W. Götz, and F. Paesani, "Comparison of permutationally invariant polynomials, neural networks, and Gaussian approximation potentials in representing water interactions through many-body expansions," *J. Chem. Phys.* **148**, 241725 (2018).
- ²⁹K. Yao, J. E. Herr, D. W. Toth, R. McKintyre, and J. Parkhill, "The TensorMol-0.1 model chemistry: a neural network augmented with long-range physics," *Chem. Sci.* **9**, 2261–2269 (2018).
- ³⁰S. Fujikake, V. L. Deringer, T. H. Lee, M. Krynski, S. R. Elliott, and G. Csányi, "Gaussian approximation potential modeling of lithium intercalation in carbon nanostructures," *J. Chem. Phys.* **148**, 241714 (2018).
- ³¹H. Li, C. Collins, M. Tanha, G. J. Gordon, and D. J. Yaron, "A Density Functional Tight Binding Layer for Deep Learning of Chemical Hamiltonians," *J. Chem. Theory Comput.* **14**, 5764–5776 (2018).
- ³²A. Grisafi, A. Fabrizio, B. Meyer, D. M. Wilkins, C. Corminboeuf, and M. Ceriotti, "Transferable machine-learning model of the electron density," *ACS Cent. Sci.* (2018), doi:10.1021/acscentsci.8b00551.
- ³³L. Zhang, J. Han, H. Wang, R. Car, and W. E, "Deep potential molecular dynamics: A scalable model with the accuracy of quantum mechanics," *Phys. Rev. Lett.* **120**, 143001 (2018).
- ³⁴R. T. McGibbon, A. G. Taube, A. G. Donchev, K. Siva, F. Hernández, C. Hargus, K.-H. Law, J. L. Klepeis, and D. E. Shaw, "Improving the accuracy of Møller-Plesset perturbation theory with neural networks," *J. Chem. Phys.* **147**, 161725 (2017).
- ³⁵M. Welborn, L. Cheng, and T. F. Miller III, "Transferability in machine learning for electronic structure via the molecular orbital basis," *J. Chem. Theory Comput.* **14**, 4772–4779 (2018).
- ³⁶G. Montavon, M. Rupp, V. Gobre, A. Vazquez-Mayagoitia, K. Hansen, A. Tkatchenko, K.-R. Müller, and O. A. von Lilienfeld, "Machine learning of molecular electronic properties in chemical compound space," *New J. Phys.* **15**, 095003 (2013).
- ³⁷L. C. Blum and J.-L. Reymond, "970 million druglike small molecules for virtual screening in the chemical universe database GDB-13," *J. Am. Chem. Soc.* **131**, 8732 (2009).
- ³⁸R. K. Nesbet, "Brueckner's theory and the method of superposition of configurations," *Phys. Rev.* **109**, 1632 (1958).
- ³⁹A. Szabo and N. S. Ostlund, *Modern Quantum Chemistry* (Dover, Mineola, 1996) pp. 231–239.
- ⁴⁰C. Möller and M. S. Plesset, "Note on an approximation treatment for many-electron systems," *Phys. Rev.* **46**, 618 (1934).
- ⁴¹G. Knizia, "Intrinsic atomic orbitals: an unbiased bridge between quantum theory and chemical concepts," *J. Chem. Theory Comput.* **9**, 4834 (2013).
- ⁴²J. Behler and M. Parrinello, "Generalized neural-network representation of high-dimensional potential-energy surfaces," *Phys. Rev. Lett.* **98**, 146401 (2007).
- ⁴³S. F. Boys, "Construction of some molecular orbitals to be approximately invariant for changes from one molecule to another," *Rev. Mod. Phys.* **32**, 296–299 (1960).
- ⁴⁴U. Kaldor, "Localized orbitals for NH_3 , C_2H_4 , and C_2H_2 ," *J. Chem. Phys.* **46**, 1981–1987 (1967).
- ⁴⁵L. Breiman, "Random forests," *Mach. Learn.* **45**, 5–32 (2001).
- ⁴⁶L. Breiman, "Statistical modeling: The two cultures," *Stat. Sci.* **16**, 199–215 (2001).
- ⁴⁷Y. Shao, Z. Gan, E. Epifanovsky, A. T. Gilbert, M. Wormit, J. Kussmann, A. W. Lange, A. Behn, J. Deng, X. Feng, D. Ghosh, M. Goldey, P. R. Horn, L. D. Jacobson, I. Kaliman, R. Z. Khaliullin, T. Kuš, A. Landau, J. Liu, E. I. Proynov, Y. M. Rhee, R. M. Richard, M. A. Rohrdanz, R. P. Steele, E. J. Sundstrom, H. L. Woodcock, P. M. Zimmerman, D. Zuev, B. Albrecht, E. Alguire, B. Austin, G. J. O. Beran, Y. A. Bernard, E. Berquist, K. Brandhorst, K. B. Bravaya, S. T. Brown, D. Casanova, C.-M. Chang, Y. Chen, S. H. Chien, K. D. Closser, D. L. Crittenden, M. Diedenhofen, R. A. DiStasio, H. Do, A. D. Dutoi, R. G. Edgar, S. Fatehi, L. Fusti-Molnar, A. Ghysels, A. Golubeva-Zadorozhnaya, J. Gomes, M. W. Hanson-Heine, P. H. Harbach, A. W. Hauser, E. G. Hohenstein, Z. C. Holden, T.-C. Jagau, H. Ji, B. Kaduk, K. Khistyayev, J. Kim, J. Kim, R. A. King, P. Klunzinger, D. Kosenkov, T. Kowalczyk, C. M. Krauter, K. U. Lao, A. D. Laurent, K. V. Lawler, S. V. Levchenko, C. Y. Lin, F. Liu, E. Livshits, R. C. Lochan, A. Luenser, P. Manohar, S. F. Manzer, S.-P. Mao, N. Mardirossian, A. V. Marenich, S. A. Maurer, N. J. Mayhall, E. Neuscamman, C. M. Oana, R. Olivares-Amaya, D. P. O'Neill, J. A. Parkhill, T. M. Perrine, R. Peverati, A. Prociuk, D. R. Rehn, E. Rosta, N. J. Russ, S. M. Sharada, S. Sharma, D. W. Small, A. Sodt, T. Stein, D. Stück, Y.-C. Su, A. J. Thom, T. Tsuchimochi, V. Vanovschi, L. Vogt, O. Vydrov, T. Wang, M. A. Watson, J. Wenzel, A. White, C. F. Williams, J. Yang, S. Yeganeh, S. R. Yost, Z.-Q. You, I. Y. Zhang, X. Zhang, Y. Zhao, B. R. Brooks, G. K. Chan, D. M. Chipman, C. J. Cramer, W. A. Goddard, M. S. Gordon, W. J. Hehre, A. Klamt, H. F. Schaefer, M. W. Schmidt, C. D. Sherrill, D. G. Truhlar, A. Warshel, X. Xu, A. Aspuru-Guzik, R. Baer, A. T. Bell, N. A. Besley, J.-D. Chai, A. Dreuw, B. D. Dunietz, T. R. Furlani, S. R. Gwaltney, C.-P. Hsu, Y. Jung, J. Kong, D. S. Lambrecht, W. Liang, C. Ochsenfeld, V. A. Rassolov, L. V. Slipchenko, J. E. Subotnik, T. Van Voorhis, J. M. Herbert, A. I. Krylov, P. M. Gill, and M. Head-Gordon, "Advances in molecular quantum chemistry contained in the Q-Chem 4 program package," *Mol. Phys.* **113**, 184 (2015).
- ⁴⁸S. H. Vosko, L. Wilk, and M. Nusair, "Accurate spin-dependent electron liquid correlation energies for local spin density calculations: a critical anal-

- ysis," *Can. J. Phys.* **58**, 1200 (1980).
- ⁴⁹C. Lee, W. Yang, and R. G. Parr, "Development of the Colle-Salvetti correlation-energy formula into a functional of the electron density," *Phys. Rev. B* **37**, 785 (1988).
- ⁵⁰A. D. Becke, "Density-functional thermochemistry. III. The role of exact exchange," *J. Chem. Phys.* **98**, 5648 (1993).
- ⁵¹P. J. Stephens, F. J. Devlin, C. F. Chabalowski, and M. J. Frisch, "Ab initio calculation of vibrational absorption and circular dichroism spectra using density functional force fields," *J. Phys. Chem.* **98**, 11623 (1994).
- ⁵²P. C. Hariharan and J. A. Pople, "The influence of polarization functions on molecular orbital hydrogenation energies," *Theor. Chim. Acta* **28**, 213 (1973).
- ⁵³G. Bussi and M. Parrinello, "Accurate sampling using Langevin dynamics," *Phys. Rev. E* **75**, 056707 (2007).
- ⁵⁴H.-J. Werner, P. J. Knowles, G. Knizia, F. R. Manby, M. Schütz, P. Celani, W. Györfy, D. Kats, T. Korona, R. Lindh, A. Mitrushenkov, G. Rauhut, K. R. Shamasundar, T. B. Adler, R. D. Amos, S. J. Bennie, A. Bernhardtsson, A. Berning, D. L. Cooper, M. J. O. Deegan, A. J. Dobbyn, F. Eckert, E. Goll, C. Hampel, A. Hesselmann, G. Hetzer, T. Hrenar, G. Jansen, C. Köppl, S. J. R. Lee, Y. Liu, A. W. Lloyd, Q. Ma, R. A. Mata, A. J. May, S. J. McNicholas, W. Meyer, T. F. Miller III, M. E. Mura, A. Nicklass, D. P. O'Neill, P. Palmieri, D. Peng, K. Pflüger, R. Pitzer, M. Reiher, T. Shiozaki, H. Stoll, A. J. Stone, R. Tarroni, T. Thorsteinsson, M. Wang, and M. Welborn, "Molpro, version 2018.3, a package of ab initio programs," (2018), see <http://www.molpro.net>.
- ⁵⁵T. H. Dunning, "Gaussian basis sets for use in correlated molecular calculations. I. The atoms boron through neon and hydrogen," *J. Chem. Phys.* **90**, 1007 (1989).
- ⁵⁶S. Saebø and P. Pulay, "Local treatment of electron correlation," *Annu. Rev. Phys. Chem.* **44**, 213–236 (1993).
- ⁵⁷J. Čížek, "On the correlation problem in atomic and molecular systems. Calculation of wavefunction components in Ursell-type expansion using quantum-field theoretical methods," *J. Chem. Phys.* **45**, 4256 (1966).
- ⁵⁸C. Hampel and H. J. Werner, "Local treatment of electron correlation in coupled cluster theory," *J. Chem. Phys.* **104**, 6286–6297 (1996).
- ⁵⁹R. J. Bartlett, J. D. Watts, S. A. Kucharski, and J. Noga, "Non-iterative fifth-order triple and quadruple excitation energy corrections in correlated methods," *Chem. Phys. Lett.* **165**, 513–522 (1990).
- ⁶⁰M. Schütz, "Low-order scaling local electron correlation methods. III. Linear scaling local perturbative triples correction (T)," *J. Chem. Phys.* **113**, 9986–10001 (2000).
- ⁶¹R. Polly, H.-J. Werner, F. R. Manby, and P. J. Knowles, "Fast Hartree-Fock theory using local density fitting approximations," *Mol. Phys.* **102**, 2311–2321 (2004).
- ⁶²C. E. Rasmussen and C. K. I. Williams, *Gaussian processes for machine learning* (MIT Press, Cambridge, MA, 2006).
- ⁶³GPY, "GPY: A gaussian process framework in python," <http://github.com/SheffieldML/GPy> (since 2012).
- ⁶⁴In principle, the smoothness of the Matérn kernel could be taken as a kernel hyperparameter; however, this possibility was not explored in this work.
- ⁶⁵F. Pedregosa, G. Varoquaux, A. Gramfort, V. Michel, B. Thirion, O. Grisel, M. Blondel, P. Prettenhofer, R. Weiss, V. Dubourg, J. Vanderplas, A. Passos, D. Cournapeau, M. Brucher, M. Perrot, and E. Duchesnay, "Scikit-learn: machine learning in python," *J. Mach. Learn. Res.* **12**, 2825 (2011).
- ⁶⁶C. Cortes, L. D. Jackel, S. A. Solla, V. Vapnik, and J. S. Denker, "Learning curves: Asymptotic values and rate of convergence," in *Advances in Neural Information Processing Systems 6*, edited by J. D. Cowan, G. Tesauro, and J. Alspector (Morgan-Kaufmann, 1994) pp. 327–334.
- ⁶⁷K. Pearson, "Mathematical contributions to the theory of evolution. III. regression, heredity, and panmixia," *Philos. Trans. R. Soc. A Math. Phys. Eng. Sci.* **187**, 253–318 (1896).
- ⁶⁸B. Kramer and A. MacKinnon, "Localization: theory and experiment," *Reports on Progress in Physics* **56**, 1469 (1993).
- ⁶⁹S. Seo, M. Wallat, T. Graepel, and K. Obermayer, "Gaussian process regression: Active data selection and test point rejection," in *Mustererkennung 2000* (Springer, 2000) pp. 27–34.
- ⁷⁰P. Zaspel, B. Huang, H. Harbrecht, and O. A. von Lilienfeld, "Boosting quantum machine learning models with multi-level combination technique: Pople diagrams revisited," *J. Chem. Theory Comput.* (2018), 10.1021/acs.jctc.8b00832.